Supplementary Information:

Frequent transitions in self-assembly across the evolution of a central metabolic enzyme

Franziska L. Sendker[1]§, Tabea Schlotthauer[1]§, Christopher-Nils Mais[2]+, Yat Kei Lo[2]+, Mathias Girbig[1], Stefan Bohn[3], Thomas Heimerl[2], Daniel Schindler[2,4], Arielle Weinstein[5], Brian P. Metzger[5], Joseph W. Thornton[5,6], Arvind Pillai[5], Gert Bange[1,2,7], Jan M. Schuller[2,7], Georg K.A. Hochberg[1,2,7]*

1 Max-Planck-Institute for Terrestrial Microbiology; Karl-von-Frisch-Str. 10, 35043 Marburg, Germany
2 Center for Synthetic Microbiology (SYNMIKRO), Philipps-University Marburg; Karl-von-Frisch-Str. 14, 35043 Marburg, Germany
3 Institute of Structural Biology, Helmholtz Center Munich, Ingolstädter Landstraße 1 Neuherberg, Germany
4 MaxGENESYS Biofoundry, Max-Planck-Institute for Terrestrial Microbiology; Karl-von-Frisch-Str. 10, 35043 Marburg, Germany
5 Department of Ecology and Evolution, University of Chicago, Chicago, IL, USA
6 Department of Human Genetics, University of Chicago, Chicago, IL, USA
7 Department of Chemistry, Philipps-University Marburg; Hans-Meerwein-Str. 4, 35043 Marburg, Germany

§ These authors contributed equally. + These authors contributed equally. * Correspondence to georg.hochberg@mpi-marburg.mpg.de

This document contains

- Supplementary Figures S1-14
- Supplementary Tables S1-4

A list of DNA sequences of all proteins used in this study is provided as Supplementary Data File 1.

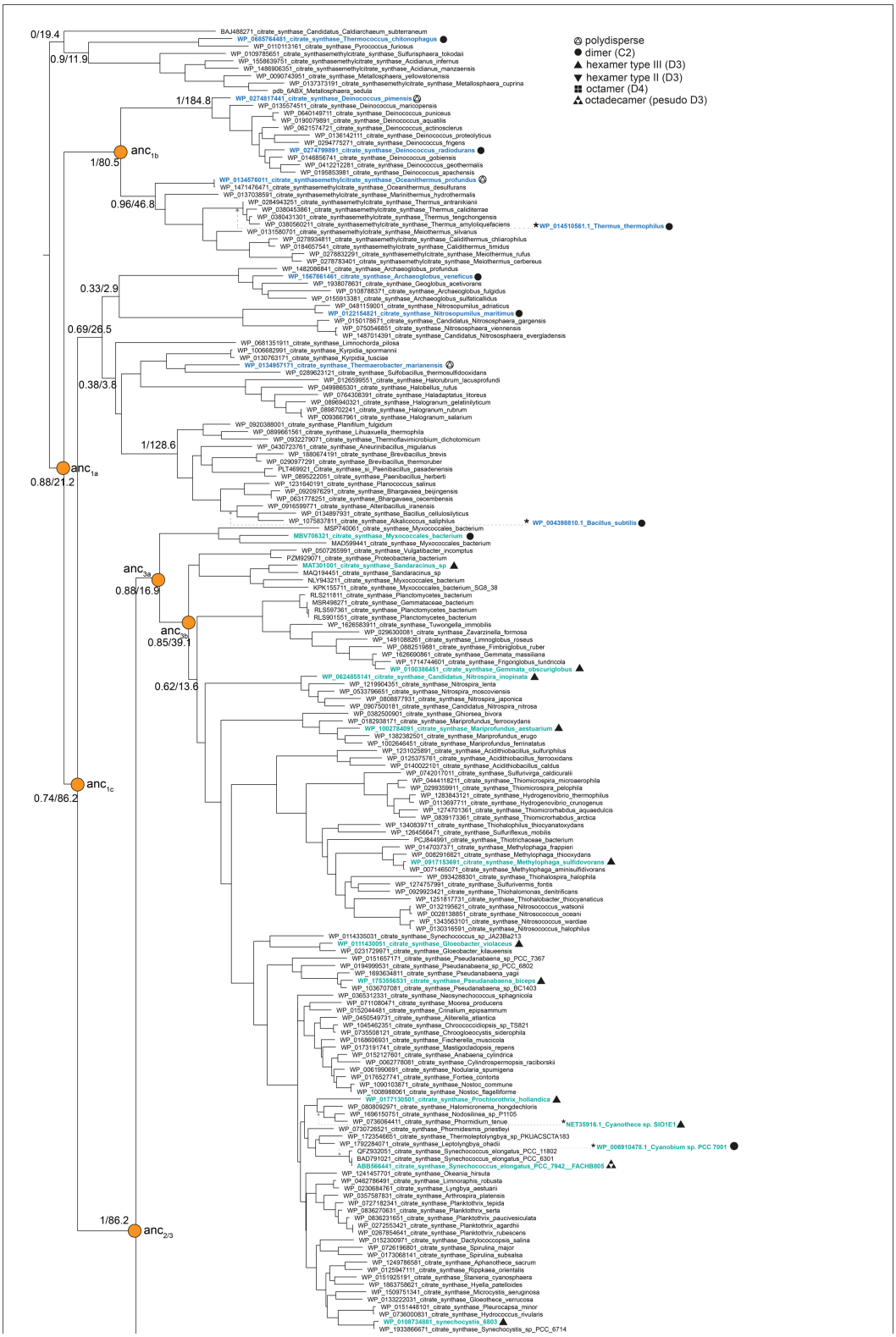
polydisperse
dimer (C2)
hexamer type III (D3)
hexamer type II (D3)
octamer (D4)
octadecamer (pesudo D3)
0/19.4
0.9/11.9
1/184.8
anc1b
1/80.5
0.96/46.8
0.33/2.9
0.69/26.5
0.38/3.8
anc1a
0.88/21.2
1/128.6
anc3a
0.88/16.9
anc3b
0.85/39.1
0.62/13.6
anc1c
0.74/86.2
1/86.2
anc2/3
BAJ48827 1_citrate_synthase_Candidatus_Caldiarchaeum_subterraneum
WP_0685764481_citrate_synthase_Thermococcus_chitonophagus
WP_0110113161_citrate_synthase_Pyrococcus_furiosus
WP_0109786561_citrate_synthasemethylcitrate_synthase_Sulfurisphaera_tokodaii
WP_1558639751_citrate_synthasemethylcitrate_synthase_Acidianus_infernus
WP_1486906351_citrate_synthasemethylcitrate_synthase_Acidianus_manzaensis
WP_0090743951_citrate_synthase_Metallosphaera_yellowstonensis
WP_0137373191_citrate_synthasemethylcitrate_synthase_Metallosphaera_cuprina
pdb_5ABX_Metallosphaera_sedula
WP_0274817441_citrate_synthase_Deinococcus_pimensis
WP_0135574511_citrate_synthase_Deinococcus_mariicopensis
WP_0640149711_citrate_synthase_Deinococcus_puniceus
WP_0190079891_citrate_synthase_Deinococcus_aquatilis
WP_0621574721_citrate_synthase_Deinococcus_actinosclerus
WP_0136142111_citrate_synthase_Deinococcus_proteolyticus
WP_0294775271_citrate_synthase_Deinococcus_frigens
WP_0274799891_citrate_synthase_Deinococcus_radiodurans
WP_0146856741_citrate_synthase_Deinococcus_gobiensis
WP_0412212281_citrate_synthase_Deinococcus_geothermalis
WP_0195853981_citrate_synthase_Deinococcus_apachensis
WP_0134576011_citrate_synthasemethylcitrate_synthase_Oceanithermus_profundus
WP_1471476471_citrate_synthasemethylcitrate_synthase_Oceanithermus_desulfurans
WP_0137038591_citrate_synthasemethylcitrate_synthase_Marinithermus_hydrothermalis
WP_0284943251_citrate_synthasemethylcitrate_synthase_Thermus_antranikianii
WP_0380453861_citrate_synthasemethylcitrate_synthase_Thermus_caldifontae
WP_0380431301_citrate_synthasemethylcitrate_synthase_Thermus_tengchongensis
WP_0380560211_citrate_synthasemethylcitrate_synthase_Thermus_amyloliquefaciens
WP_014510561.1_Thermus_thermophilus
WP_0131580701_citrate_synthasemethylcitrate_synthase_Meiothermus_silvanus
WP_0278934811_citrate_synthasemethylcitrate_synthase_Calidithermus_chliarophilus
WP_0184657541_citrate_synthasemethylcitrate_synthase_Calidithermus_timidus
WP_0278832291_citrate_synthasemethylcitrate_synthase_Meiothermus_rufus
WP_0278783401_citrate_synthasemethylcitrate_synthase_Meiothermus_cerbereus
WP_1482088841_citrate_synthase_Archaeoglobus_profundus
WP_1567861461_citrate_synthase_Archaeoglobus_veneficus
WP_1938078631_citrate_synthase_Geoglobus_acetivorans
WP_0108788371_citrate_synthase_Archaeoglobus_fulgidus
WP_0155913381_citrate_synthase_Archaeoglobus_sulfaticallidus
WP_0481159001_citrate_synthase_Nitrosopumilus_adriaticus
WP_0122154821_citrate_synthase_Nitrosopumilus_maritimus
WP_0150178671_citrate_synthase_Candidatus_Nitrososphaera_gargensis
WP_0750546851_citrate_synthase_Nitrososphaera_viennensis
WP_1487014391_citrate_synthase_Candidatus_Nitrososphaera_evergladensis
WP_0681351911_citrate_synthase_Limnochorda_pilosa
WP_1006682991_citrate_synthase_Kyrpidia_spormannii
WP_0130763171_citrate_synthase_Kyrpidia_tusciae
WP_0134957171_citrate_synthase_Thermaerobacter_marianensis
WP_0289623121_citrate_synthase_Sulfobacillus_thermosulfidooxidans
WP_0126599551_citrate_synthase_Halorubrum_lacusprofundi
WP_0499865301_citrate_synthase_Halobellus_rufus
WP_0764308391_citrate_synthase_Haladaptatus_litoreus
WP_0896940321_citrate_synthase_Halogranum_gelatinilyticum
WP_0898702241_citrate_synthase_Halogranum_rubrum
WP_0093667961_citrate_synthase_Halogranum_salarium
WP_0920388001_citrate_synthase_Planifilum_fulgidum
WP_0899661561_citrate_synthase_Lihuaxuella_thermophila
WP_0932279071_citrate_synthase_Thermoflavimicrobium_dichotomicum
WP_0430723761_citrate_synthase_Anaurinibacillus_migulanus
WP_1880674191_citrate_synthase_Brevibacillus_brevis
WP_0290977291_citrate_synthase_Brevibacillus_thermoruber
PLT469921_Citrate_synthase_si_Paenibacillus_pasadenensis
WP_0895222051_citrate_synthase_Paenibacillus_herberti
WP_1231640191_citrate_synthase_Planococcus_salinus
WP_0920976291_citrate_synthase_Bhargavaea_beijingensis
WP_0631778251_citrate_synthase_Bhargavaea_cecembensis
WP_0916599771_citrate_synthase_Alteribacillus_iranensis
WP_0134897931_citrate_synthase_Bacillus_cellulosilyticus
WP_1075837811_citrate_synthase_Alkalicoccus_saliphilus
WP_004398810.1_Bacillus_subtilis
MSP740061_citrate_synthase_Myxococcales_bacterium
MBV706321_citrate_synthase_Myxococcales_bacterium
MAD599441_citrate_synthase_Myxococcales_bacterium
WP_0507265991_citrate_synthase_Vulgatibacter_incomptus
PZM929071_citrate_synthase_Proteobacteria_bacterium
MAT301001_citrate_synthase_Sandaracinus_sp
MAQ194451_citrate_synthase_Sandaracinus_sp
NLY943211_citrate_synthase_Myxococcales_bacterium
KPK155711_citrate_synthase_Myxococcales_bacterium_SG8_38
RLS211811_citrate_synthase_Planctomycetes_bacterium
MSR498271_citrate_synthase_Gemmataceae_bacterium
RLS597361_citrate_synthase_Planctomycetes_bacterium
RLS901551_citrate_synthase_Planctomycetes_bacterium
WP_1626583911_citrate_synthase_Tuwongella_immobilis
WP_0296300081_citrate_synthase_Zavarzinella_formosa
WP_1491088261_citrate_synthase_Limnoglobus_roseus
WP_0882519881_citrate_synthase_Fimbriiglobus_ruber
WP_1626690861_citrate_synthase_Gemmata_massiliana
WP_1714744601_citrate_synthase_Frigoriglobus_tundricola
WP_0100386451_citrate_synthase_Gemmata_obscuriglobus
WP_0624855141_citrate_synthase_Candidatus_Nitrospira_inopinata
WP_1219904351_citrate_synthase_Nitrospira_lenta
WP_0533706651_citrate_synthase_Nitrospira_moscoviensis
WP_0808877851_citrate_synthase_Nitrospira_japonica
WP_0907500181_citrate_synthase_Candidatus_Nitrospira_nitrosa
WP_0382500901_citrate_synthase_Ghiorsea_bivora
WP_0182938171_citrate_synthase_Mariprofundus_ferrooxydans
WP_1002784091_citrate_synthase_Mariprofundus_aestuarium
WP_1382382501_citrate_synthase_Mariprofundus_erugo
WP_1002646451_citrate_synthase_Mariprofundus_ferrinatatus
WP_1231025891_citrate_synthase_Acidithiobacillus_sulfuriphilus
WP_0125375761_citrate_synthase_Acidithiobacillus_ferrooxidans
WP_0140022101_citrate_synthase_Acidithiobacillus_caldus
WP_0742017011_citrate_synthase_Sulfurivirga_caldicuralii
WP_0444118211_citrate_synthase_Thiomicrospira_microaerophila
WP_0299359911_citrate_synthase_Thiomicrospira_pelophila
WP_1283843121_citrate_synthase_Hydrogenovibrio_thermophilus
WP_0113697711_citrate_synthase_Hydrogenovibrio_crunogenus
WP_1274701361_citrate_synthase_Thiomicrorhabdus_aquaedulcis
WP_0839173361_citrate_synthase_Thiomicrorhabdus_arctica
WP_1340839711_citrate_synthase_Thiohalophilus_thiocyanatoxydans
WP_1264566471_citrate_synthase_Sulfuriflexus_mobilis
PCJ844991_citrate_synthase_Thiotrichaceae_bacterium
WP_0147037371_citrate_synthase_Methylophaga_frappieri
WP_0082916621_citrate_synthase_Methylophaga_thiooxydans
WP_0917153691_citrate_synthase_Methylophaga_sulfidovorans
WP_0071465071_citrate_synthase_Methylophaga_aminisulfidivorans
WP_0934288301_citrate_synthase_Thiohalospira_halophila
WP_1274757991_citrate_synthase_Sulfurivermis_fontis
WP_0929923421_citrate_synthase_Thiohalomonas_denitrificans
WP_1251817731_citrate_synthase_Thiohalobacter_thiocyanaticus
WP_0132195621_citrate_synthase_Nitrosococcus_watsonii
WP_0028138851_citrate_synthase_Nitrosococcus_oceani
WP_1343563101_citrate_synthase_Nitrosococcus_wardiae
WP_0130316591_citrate_synthase_Nitrosococcus_halophilus
WP_0114335031_citrate_synthase_Synechococcus_sp_JA23Ba213
WP_0111430051_citrate_synthase_Gloeobacter_violaceus
WP_0231729971_citrate_synthase_Gloeobacter_kilaueensis
WP_0151657171_citrate_synthase_Pseudanabaena_sp_PCC_7367
WP_0194999531_citrate_synthase_Pseudanabaena_sp_PCC_6802
WP_1693634811_citrate_synthase_Pseudanabaena_yagii
WP_1753556531_citrate_synthase_Pseudanabaena_biceps
WP_1036707081_citrate_synthase_Pseudanabaena_sp_BC1403
WP_0365312331_citrate_synthase_Neosynechococcus_sphagnicola
WP_0711080471_citrate_synthase_Moorea_producens
WP_0152044481_citrate_synthase_Crinalium_epipsammum
WP_0450549731_citrate_synthase_Alterella_atlantica
WP_1045462351_citrate_synthase_Chroococcidiopsis_sp_TS821
WP_0735508121_citrate_synthase_Chroogloeocystis_siderophila
WP_0168606931_citrate_synthase_Fischerella_muscicola
WP_0173191741_citrate_synthase_Mastigocladopsis_repens
WP_0152127901_citrate_synthase_Anabaena_cylindrica
WP_0062778081_citrate_synthase_Cylindrospermopsis_raciborskii
WP_0061990691_citrate_synthase_Nodularia_spumigena
WP_0176527741_citrate_synthase_Fortiea_contorta
WP_1090103871_citrate_synthase_Nostoc_commune
WP_1008988061_citrate_synthase_Nostoc_flagelliforme
WP_0177130501_citrate_synthase_Prochlorothrix_hollandica
WP_0808092971_citrate_synthase_Halomicronema_hongdechloris
WP_1696150751_citrate_synthase_Nodosilinea_sp_P1105
WP_0736064411_citrate_synthase_Phormidium_tenue
NET35916.1_Cyanothece sp. SIO1E1
WP_0730726521_citrate_synthase_Phormidesmis_priestleyi
WP_1723546851_citrate_synthase_Thermoleptolyngbya_sp_PKUACSCTA183
WP_1792284071_citrate_synthase_Leptolyngbya_ohadii
WP_006910478.1_Cyanobium sp. PCC 7001
QFZ932051_citrate_synthase_Synechococcus_elongatus_PCC_11802
BAD791021_citrate_synthase_Synechococcus_elongatus_PCC_6301
ABB566441_citrate_synthase_Synechococcus_elongatus_PCC_7942__FACHB805
WP_1241457701_citrate_synthase_Okeania_hirsuta
WP_0462786491_citrate_synthase_Limnoraphis_robusta
WP_0230684761_citrate_synthase_Lyngbya_aestuarii
WP_0357587831_citrate_synthase_Arthrospira_platensis
WP_0727182341_citrate_synthase_Planktothrix_tepida
WP_0836270631_citrate_synthase_Planktothrix_serta
WP_0836231651_citrate_synthase_Planktothrix_paucivesiculata
WP_0272553421_citrate_synthase_Planktothrix_agardhii
WP_0267854641_citrate_synthase_Planktothrix_rubescens
WP_0152300971_citrate_synthase_Dactylococcopsis_salina
WP_0726196801_citrate_synthase_Spirulina_major
WP_0173068141_citrate_synthase_Spirulina_subsalsa
WP_1249786581_citrate_synthase_Aphanothece_sacrum
WP_0125947111_citrate_synthase_Ripkaea_orientalis
WP_0151925191_citrate_synthase_Stanieria_cyanosphaera
WP_1863756621_citrate_synthase_Hyella_patelloides
WP_1509751341_citrate_synthase_Microcystis_aeruginosa
WP_0133222031_citrate_synthase_Gloeothece_verrucosa
WP_0151448101_citrate_synthase_Pleurocapsa_minor
WP_0736000831_citrate_synthase_Hydrococcus_rivularis
WP_0108734881_synechocystis_6803
WP_1933866671_citrate_synthase_Synechocystis_sp_PCC_6714

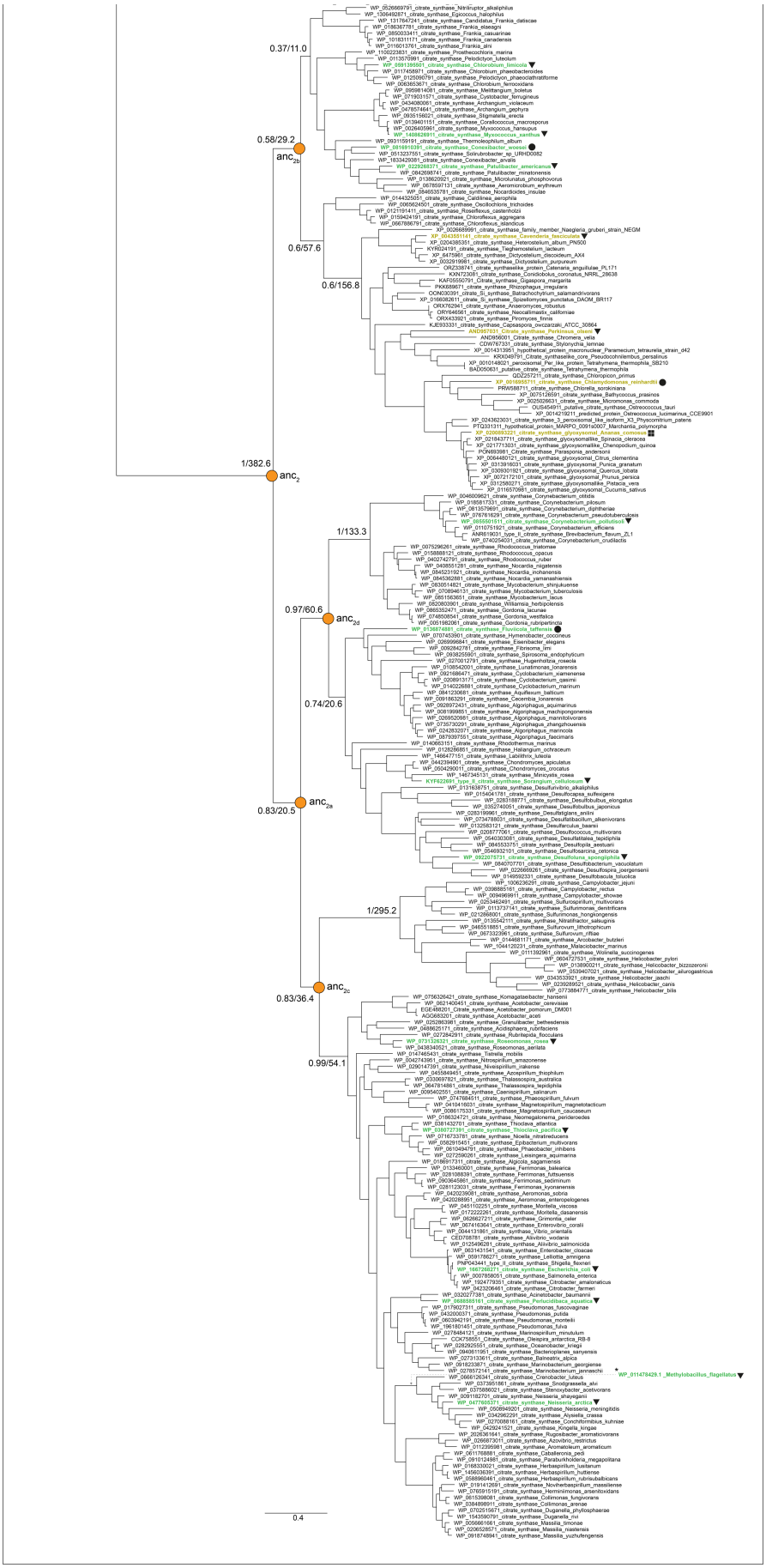
0.37/11.0
0.58/29.2
anc2b
0.6/57.6
0.6/156.8
1/382.6
anc2
1/133.3
0.97/60.6
anc2d
0.74/20.6
anc2a
0.83/20.5
1/295.2
anc2c
0.83/36.4
0.99/54.1
0.4

Supplementary Fig. 1 Phylogenetic tree of citrate synthase Full tree with all sequences (organism name and NCBI-identifier) to infer the evolutionary history of citrate synthase (CS) in Bacteria, Archaea and non-mitochondrial CS in Eukaryotes. Extant sequences that were purified are colored and their quaternary structure is indicated with a symbol. Internal nodes of the tree for which ancestral sequences were reconstructed via ancestral sequence reconstruction (ASR) are indicated. Branch supports values are shown for these nodes and additional important internal branches as Felsenstein's bootstrap values and approximate likelihood ratio test statistics (fbe/aLRT). Four sequences of characterized extant CS were not included in the inference of the main phylogeny used for ASR. Their position on the tree was inferred afterwards by recalculating the phylogeny and is indicated with dashed lines.

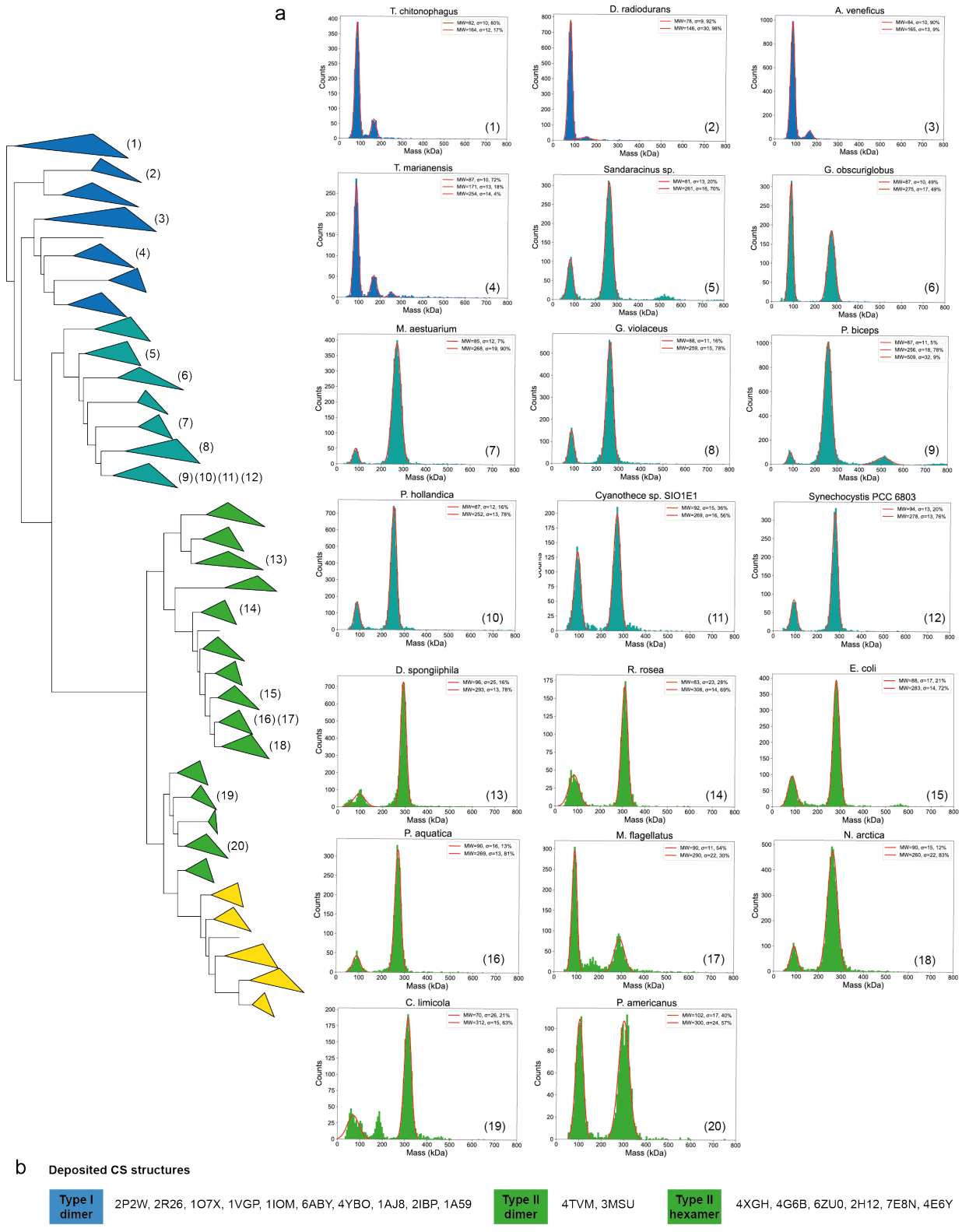

Supplementary Fig. 2 Mass photometry measurements of additional characterized extant citrate synthase (a) Mass photometry histograms of additional purified extant citrate synthases

(CS) and their respective position on the inferred phylogenetic tree. (b) PDB accession codes of previously characterized and deposited structures of prokaryotic CS. Source data are provided as a Source Data file.

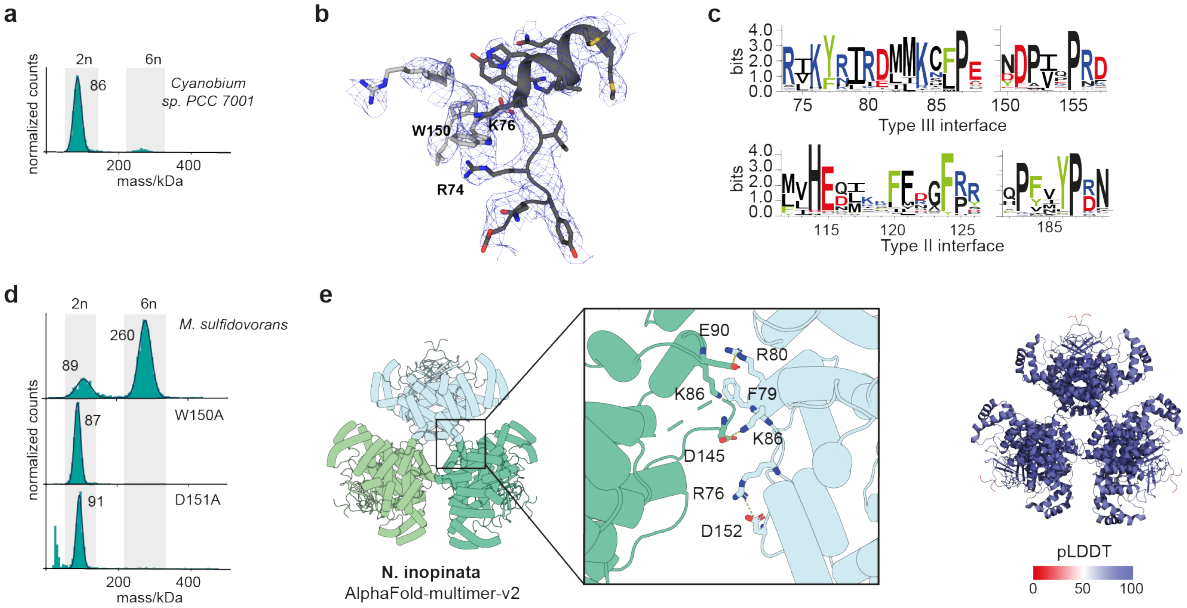

Supplementary Fig. 3 Important residues for type III hexamer formation (a) Mass photometry (MP) measurement of the dimeric type III citrate synthase (CS) from *Cyanobium* sp. PCC 7001. (b) Electron density map of the crystal structure of the CS from *M. sulfidovorans* at the interface of two subunits (compare Fig. 2d). The $2F_{obs}$-F_{calc} after final refinement is shown as a blue mesh at 1 σ. Protein is represented as cartoon with side chains as sticks. (c) Sequence logo of amino acid residues that are found within the interface of type II or III CS, demonstrating strong differences. Homologous sites are aligned, shift in site numbers results from a longer N-terminus in type II CS. (d) MP measurement of interface variants of the type III CS from *M. sulfidovorans*. (e) Structural prediction of the hexameric type III CS from *N. inopinata* inferred with AlphaFold-multimer-v2 with close up of the interface between dimers. Right: structural model colored according to the predicted local distance difference test (pLDDT). Source data are provided as a Source Data file.

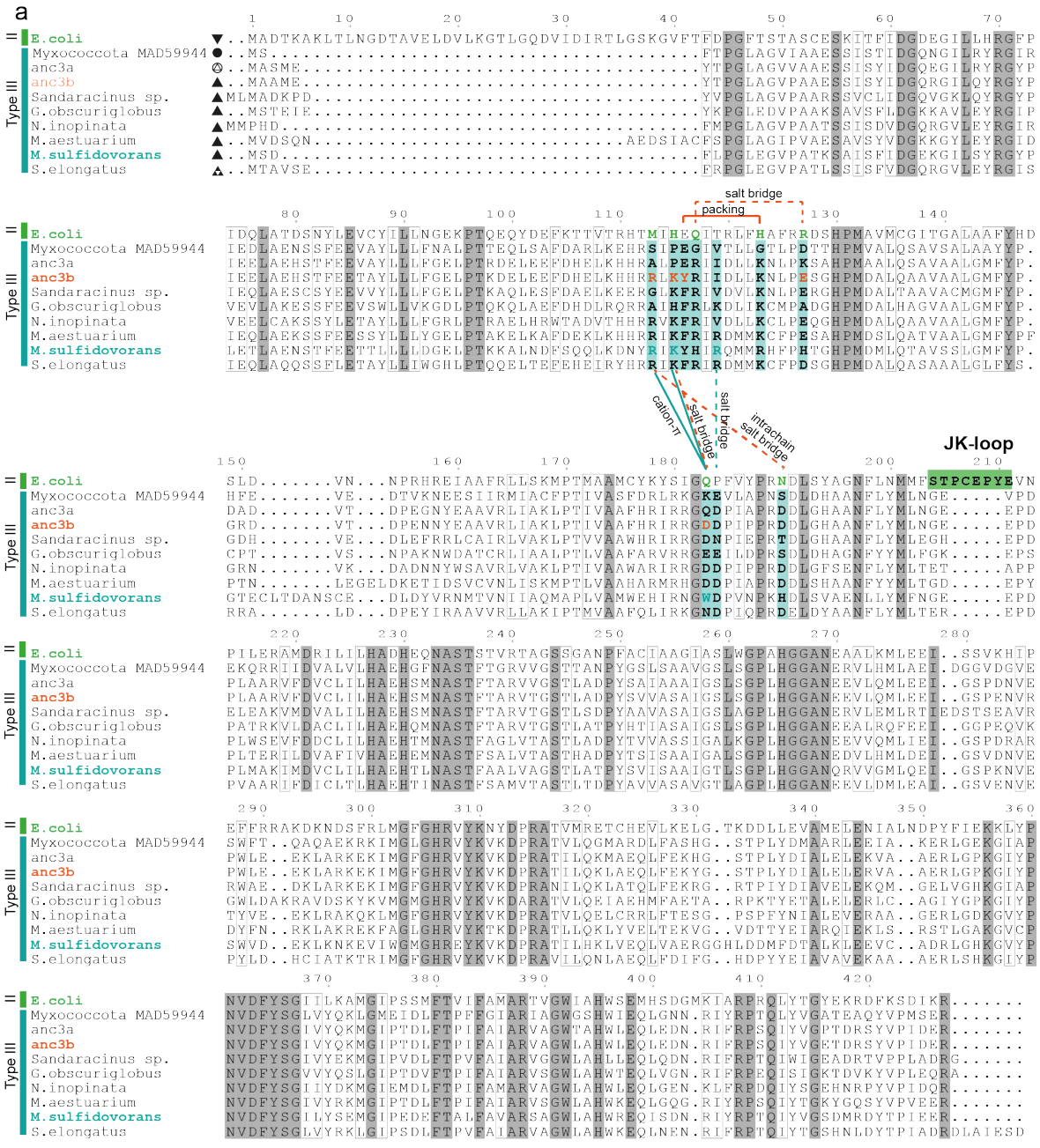

Supplementary Fig. 4 Conservation of residues inducing hexameric assembly in type III citrate synthase. Alignment of characterized type III citrate synthases (CS), ancestors anc_{3a}, anc_{3b} and the type II CS from *E. coli*. Residues marked in teal are part of the hexamer interface in type III enzymes. Connecting lines indicate direct interactions between residues in structures (teal=*M. sulfidovorans*, orange=anc_{3b}). Residues that take part in the hexamer formation in *E. coli* CS are colored in green.

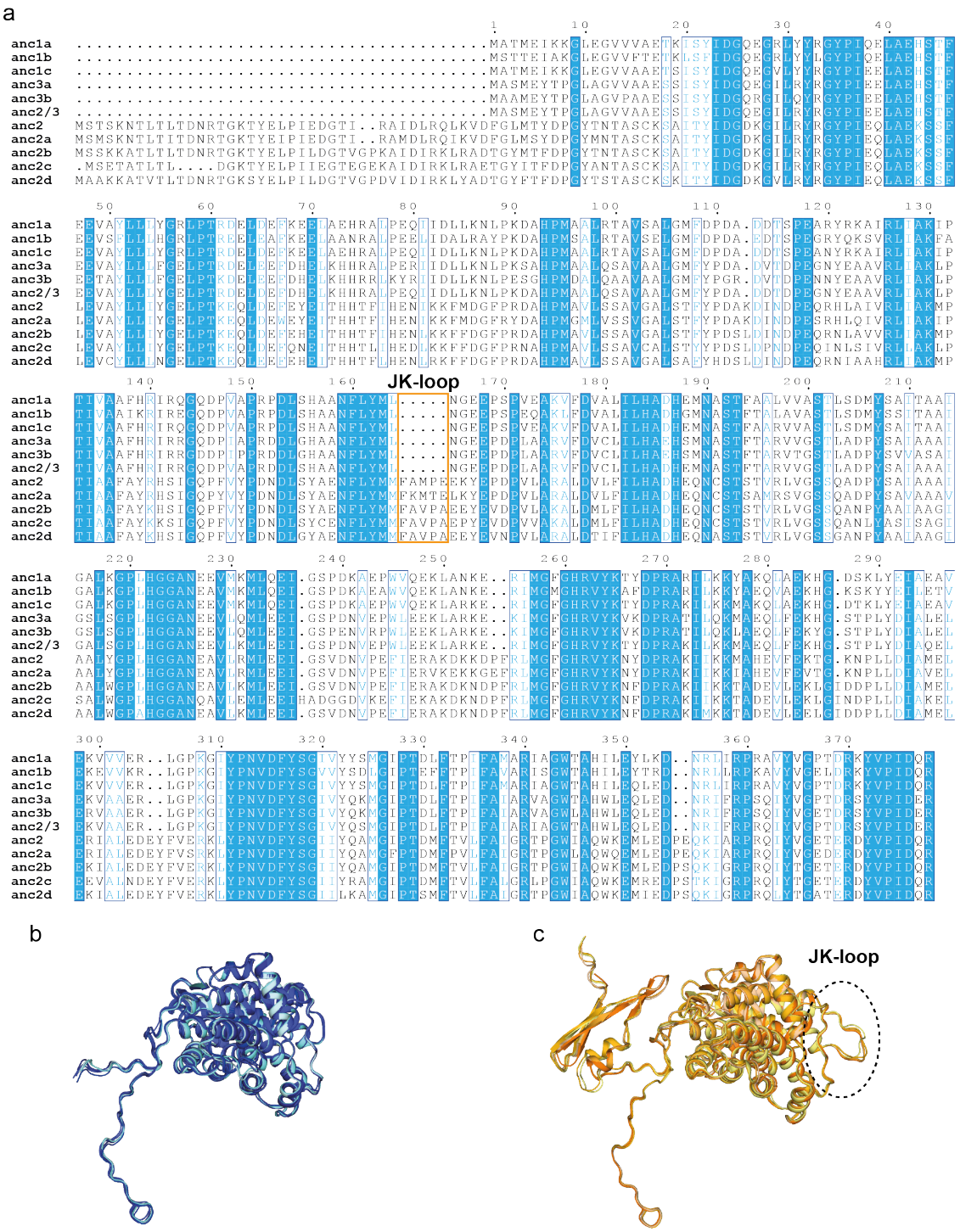

Supplementary Fig. 5 Sequences and predicted structures of reconstructed ancestral citrate synthase sequences (a) Alignment of the amino acid sequences of the inferred ancestral proteins. (b) Aligned Alphafold2 predictions of monomeric ancestral citrate synthase (CS) anc_{1a},

anc_{1b}, anc_{1c}, $anc_{2/3}$, anc_{3a} and anc_{3b}. (c) Aligned Alphafold2 predictions of monomeric ancestral CS anc_2, anc_{2a}, anc_{2b}, anc_{2c} and anc_{2d}.

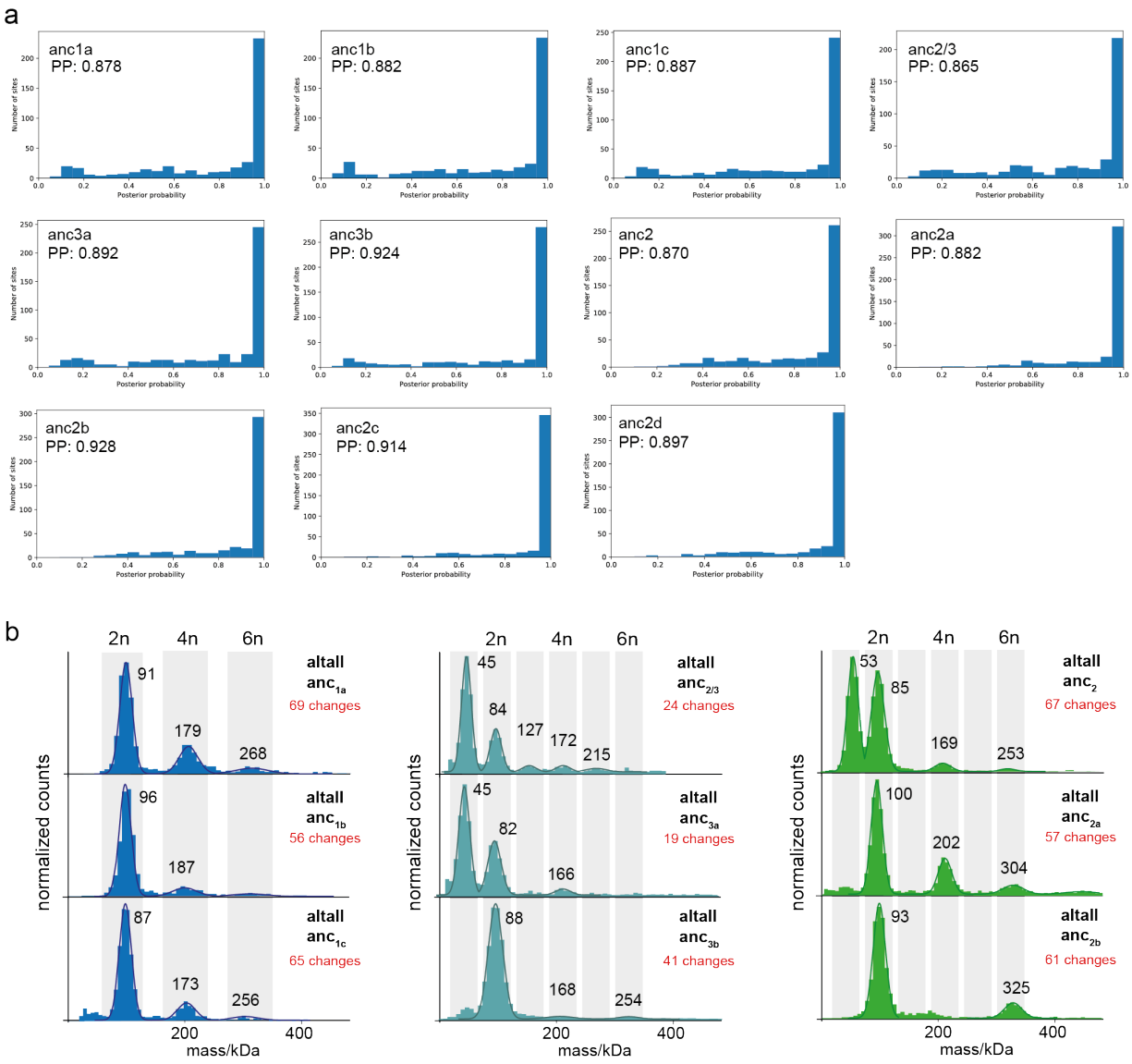

Supplementary Fig. 6 Robustness of the inferred ancestral proteins (a) Histograms per-site of the posterior probabilities (PP) of the maximum aposteriori state across reconstructed sites for all eleven ancestral proteins. (b) Mass photometry measurements of purified alternative ancestral proteins (altall = all position changed to the second most likely amino acid, if PP >0.2 and for altall $anc_{2/3}$ and anc_{3a} if PP >0.3). Number of changes denotes the differences to the maximum-likelihood ancestral sequence. Source data are provided as a Source Data file.

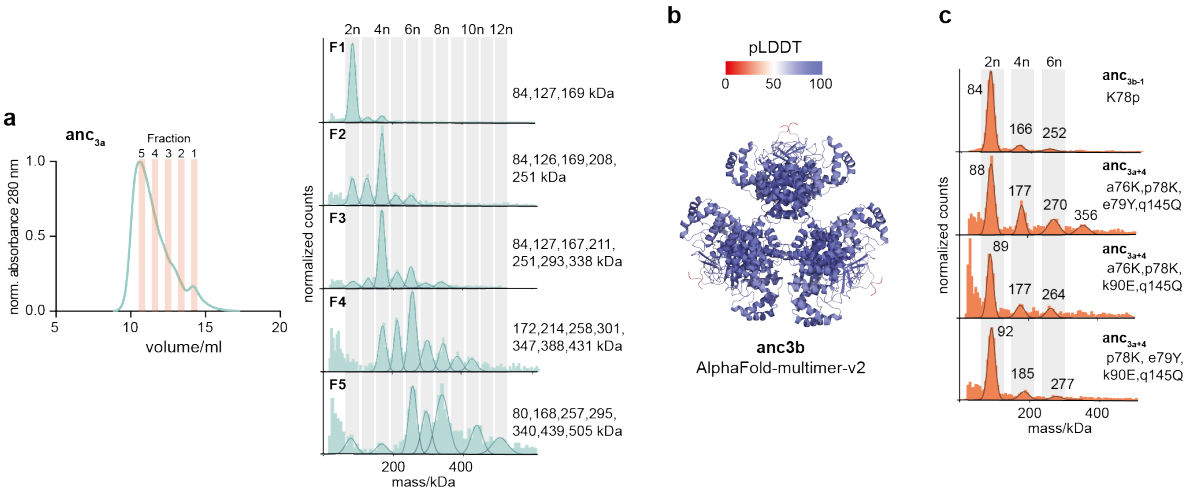

Supplementary Fig. 7 Type III ancestors assemble into polydisperse distributions (a) Size exclusion chromatography trace of the polydisperse anc_{3a} and mass photometry (MP) measurements of the isolated fractions. (b) MP measurements of variants of anc_{3a} with different combinations of substitutions that emerged in the interval to anc_{3b} (small and capital letters indicate the ancestral and derived amino acid, respectively). No combination of 4 was sufficient to induce hexameric assembly. The significance of the substitution p78K was shown by a reversal (K78p) in the hexameric anc_{3b}. (c) AlphaFold-multimer prediction of anc3b color-coded according to the site-wise pLDDT score. Source data are provided as a Source Data file.

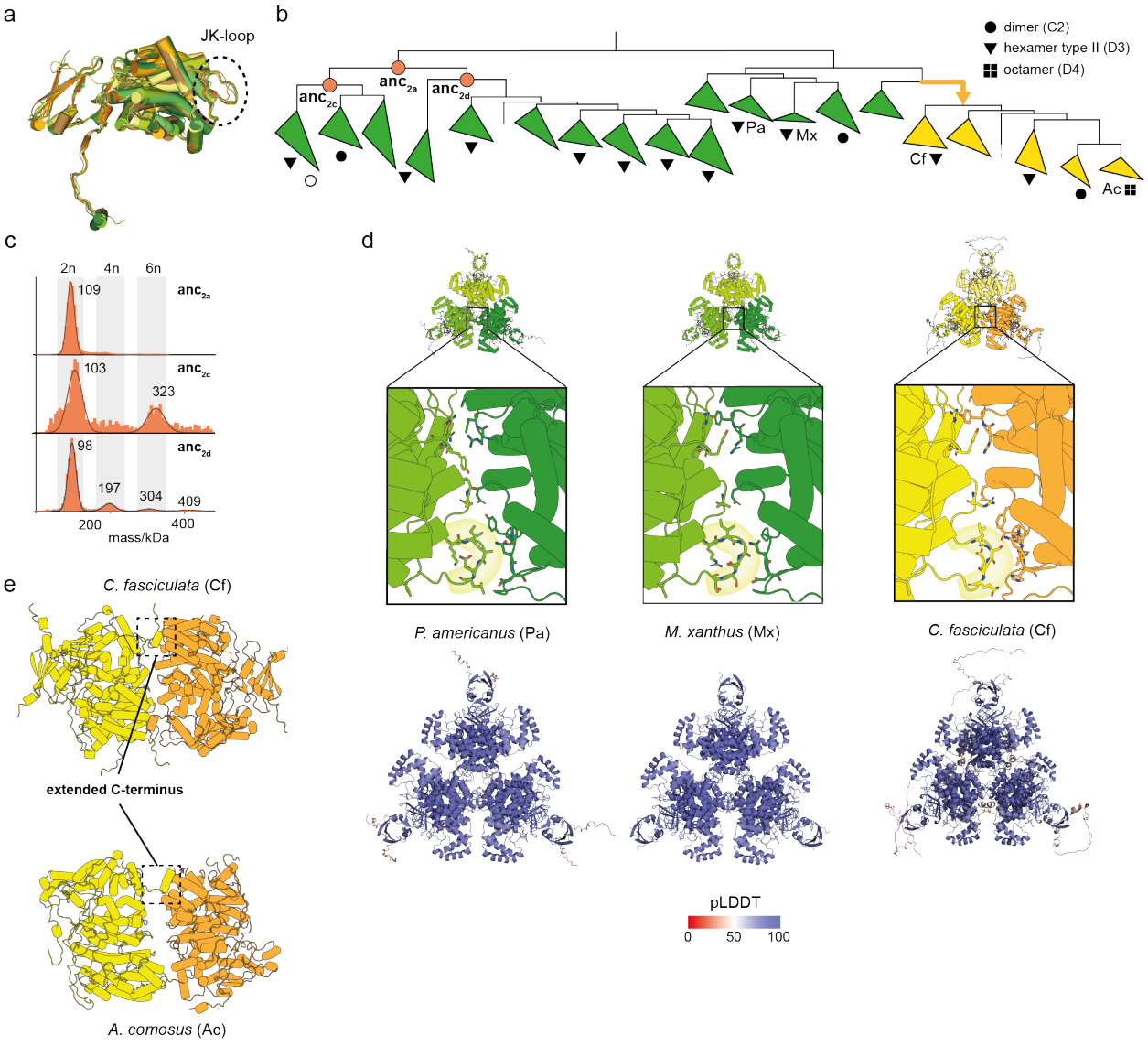

Supplementary Fig. 8 Inconclusive inference of the emergence of type II hexamers but conserved involvement of the JK-loop (a) Structural alignment of deposited type II citrate synthases (CS). All have the JK-loop (PDB: 4E6Y, 6ZU0, 2H12, 4G6B, 4XGH, 7E8N, 4TVM, 3MSU). (b) Schematic representation of part of the CS phylogeny displaying the quaternary structures of characterized type II CS. Nodes corresponding to resurrected ancestral CS are indicated (orange circles). (c) Mass photometry measurements of anc_{2a} and its descendants anc_{2c} and anc_{2d}. (d) Upper: AlphaFold-Multimer predictions of hexameric type II CS and non-mitochondrial CS with close ups on the interface that display the involvement of the JK-loop for all of them. Lower: pLDDT-colored structures of the same models. (e) Comparison of the extended C-terminus in the hexameric structure from *C. fasiculata* (AlphaFold-Multimer prediction) and octameric structure from *A. comosus* (cryo-EM). Only two dimers are displayed

for both structures to highlight the cross-connection by the C-terminus between adjacent dimers. Source data are provided as a Source Data file.


nmCS
Type II
JK-loop
extended C-terminus

Supplementary Fig. 9 Conservation of residues inducing oligomeric assembly in type II citrate synthases (CS) and non-mitochondrial CS. Alignment of the characterized type II CS and nmCS. Residues marked in green take part in the hexamer formation in the hexamer from *E. coli*. The extended C-terminus of nmCS is colored in yellow.

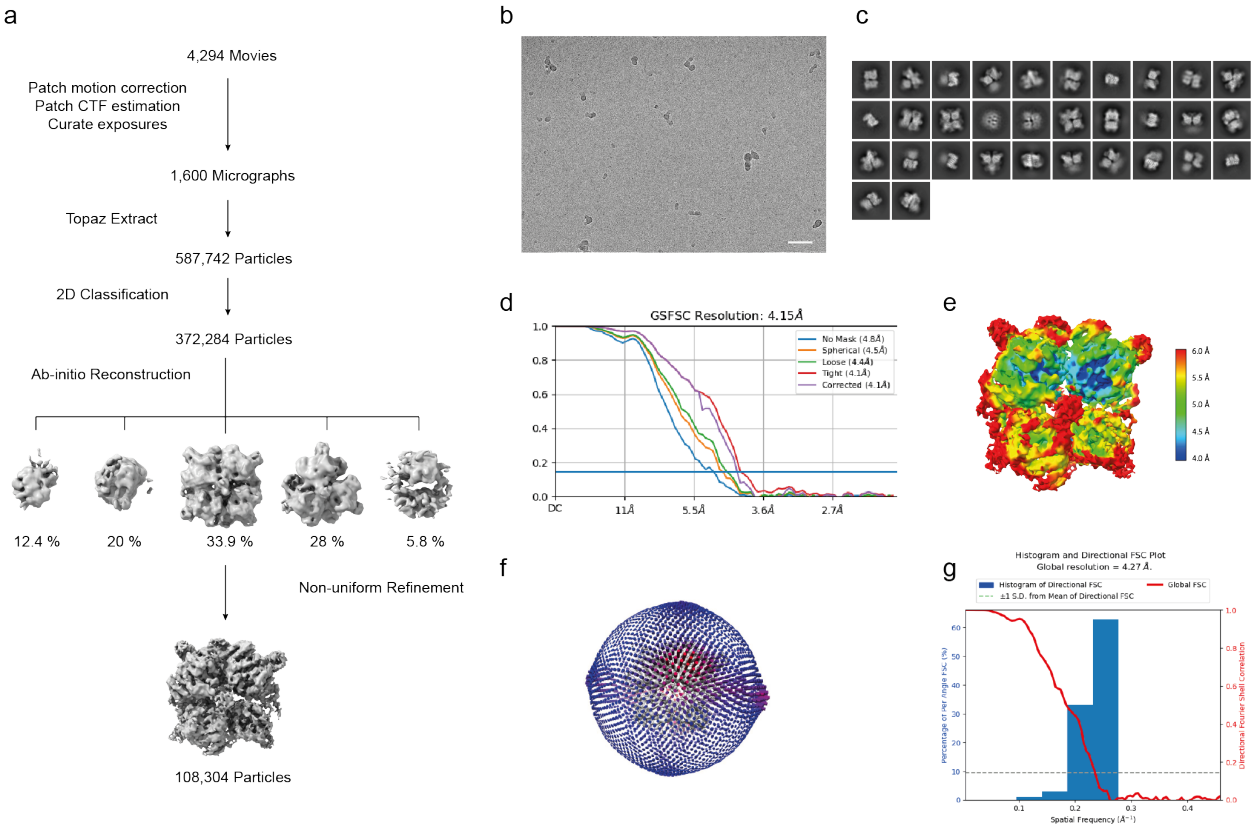

Supplementary Fig. 10 Cryo-EM data processing. (a) An overview of the image processing procedure (see Methods). (b) A representative micrograph of *A. cosmosus* CS acquired from FEI Titan Kriso (scale bar, 50 nm). (c) 2D classes selected for ab-initio reconstruction. (d) Fourier shell correlation (FSC) curves for the reconstruction applying different masks. (e) The final density map colored by local resolution. (f) Euler angular distribution of particles used in the final 3D reconstruction. (g) The histogram of directional FSC.

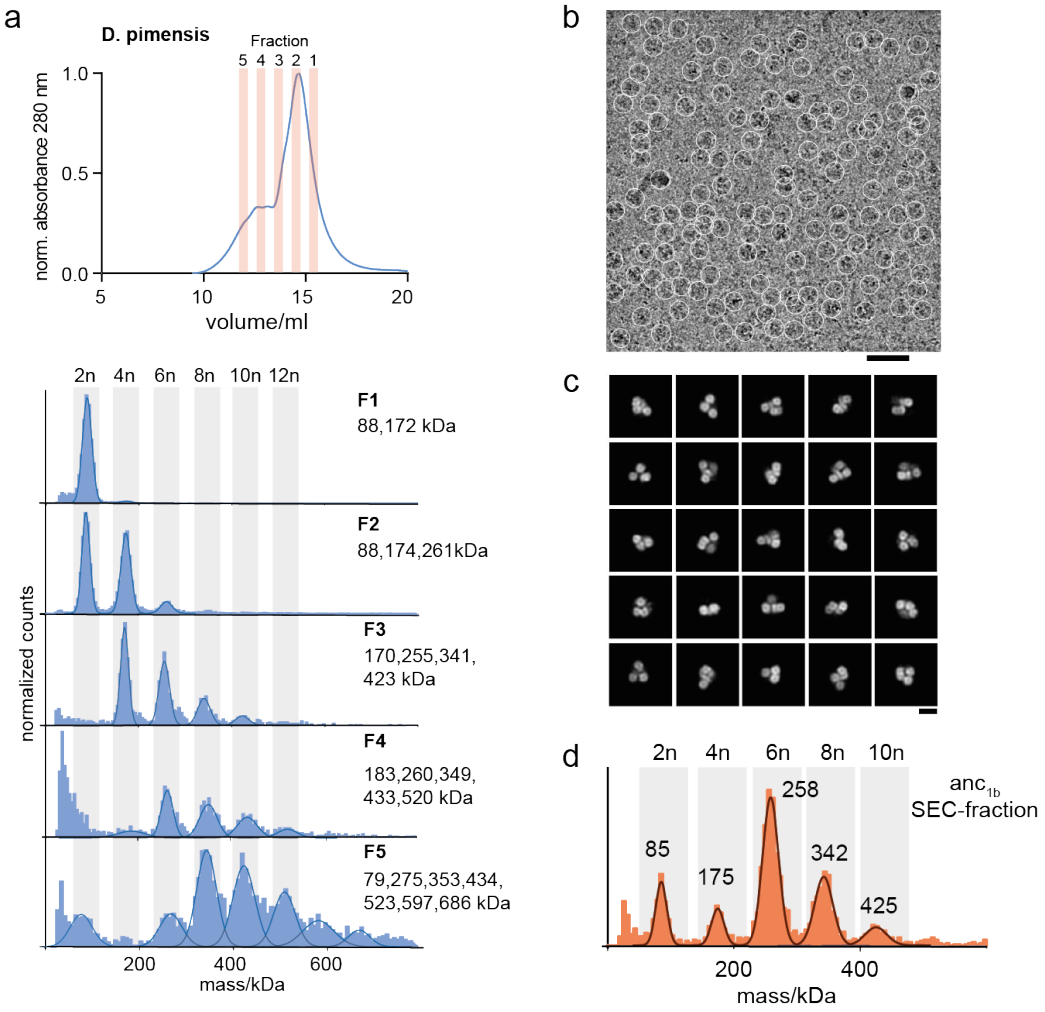

Supplementary Fig. 11 Polydisperse type I enzymes form multiples of dimers (a) Size exclusion chromatography (SEC) trace of polydisperse citrate synthase (CS) from *D. pimensis* and mass photometry (MP) measurements of the isolated fractions. (b) Exemplary cryo-EM micrograph of oligomeric complexes of polydisperse anc_{1a}, low-pass filtered at 5 Å. Particle picks are depicted as white circles (diameter = 180 Å). Scale bar = 40 nm. (c) 2D class averages of polydisperse anc_{1a}. Scale bar = 10 nm. (d) MP measurement of the SEC-fraction used for cryo-EM. Source data are provided as a Source Data file.

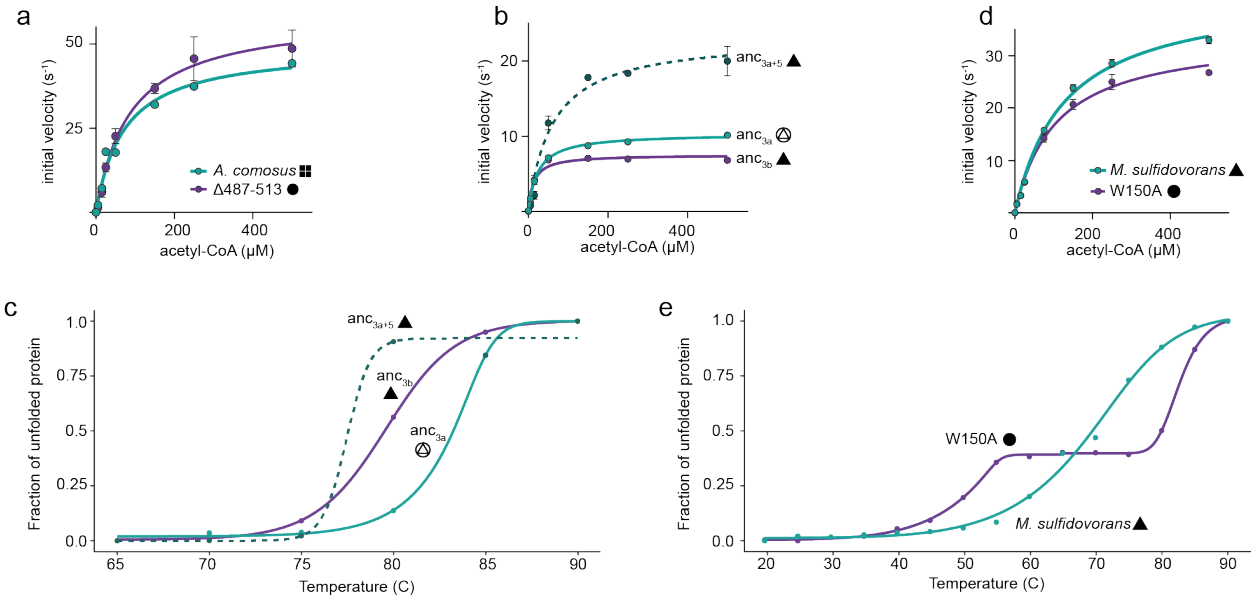

Supplementary Fig. 12 Kinetic measurements with saturated oxaloacetate and thermal stability (a) Michaelis-Menten kinetics of extant citrate synthase (CS) from *A. comosus* and a variant that disrupts interfaces between dimeric subcomplexes and prevent assembly into larger oligomers (Δ487-513). Data are presented as mean values +/- SD, n = 3 technical replicates. (b) Michaelis-Menten kinetics of the ancestral CS bracketing the emergence of hexamers within type III enzymes (anc_{3a}, anc_{3b}) and the minimal substitution construct to yield hexameric complexes (anc_{3a+5}). Data are presented as mean values +/- SD, n = 3 technical replicates. (c) Thermal stability measurements of the ancestral CS (anc_{3a}, anc_{3b}, anc_{3a+5}) using circular dichroism to evaluate folding of the protein. (d) Michaelis-Menten kinetics of extant CS from *M. sulfidovorans* and a variant that disrupts interfaces between dimeric subcomplexes and prevent assembly into larger oligomers (W150A). Data are presented as mean values +/- SD, n = 3 technical replicates. (e) Thermal stability measurements of the extant CS *M. sulfidovorans* and a variant that disrupts interfaces between dimeric subcomplexes and prevent assembly into larger oligomers (W150A) using circular dichroism to evaluate folding of the protein. Source data are provided as a Source Data file.

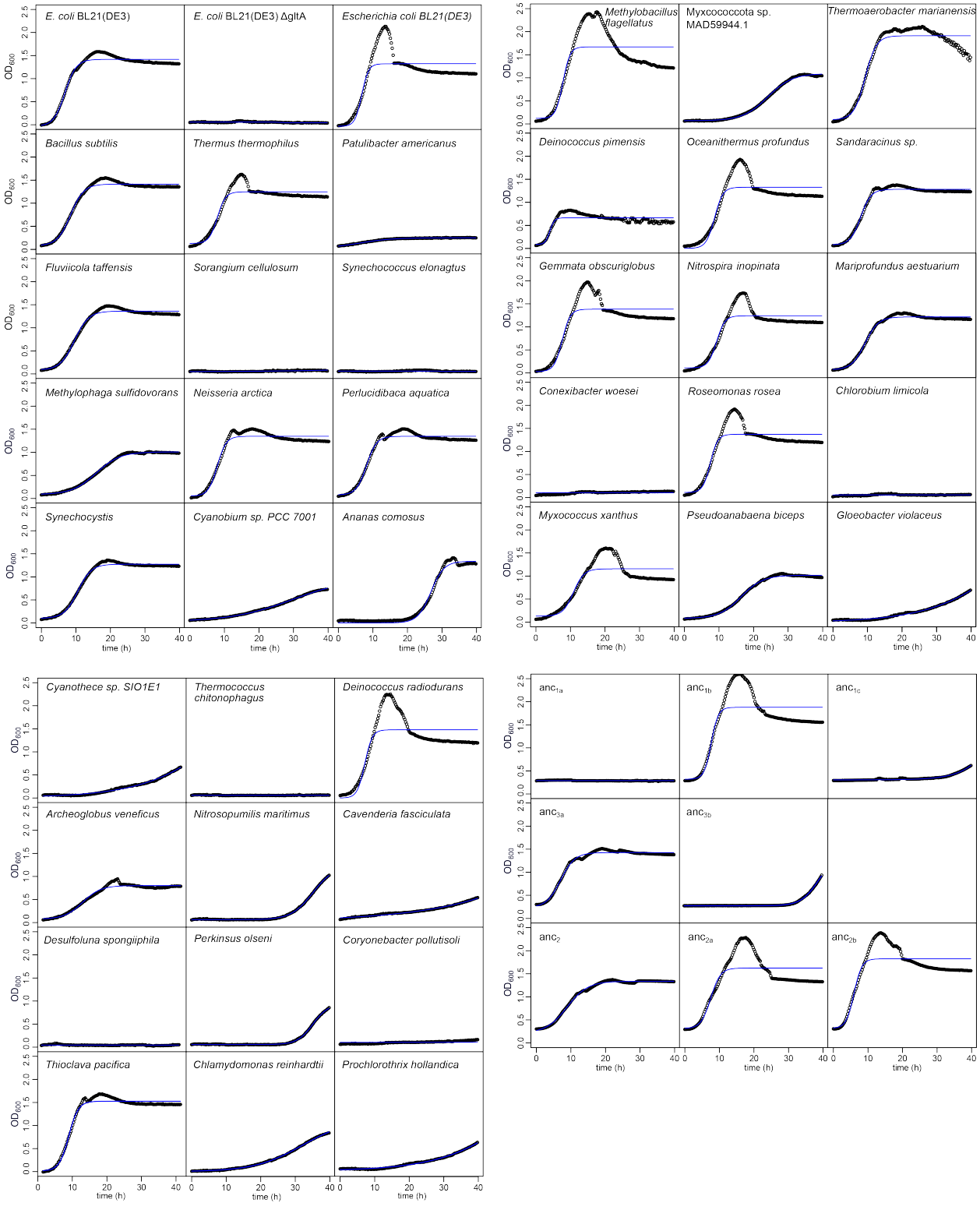

Supplementary Fig. 13 Growth data of complemented strains with fitted growth curves

Source data are provided as a Source Data file.

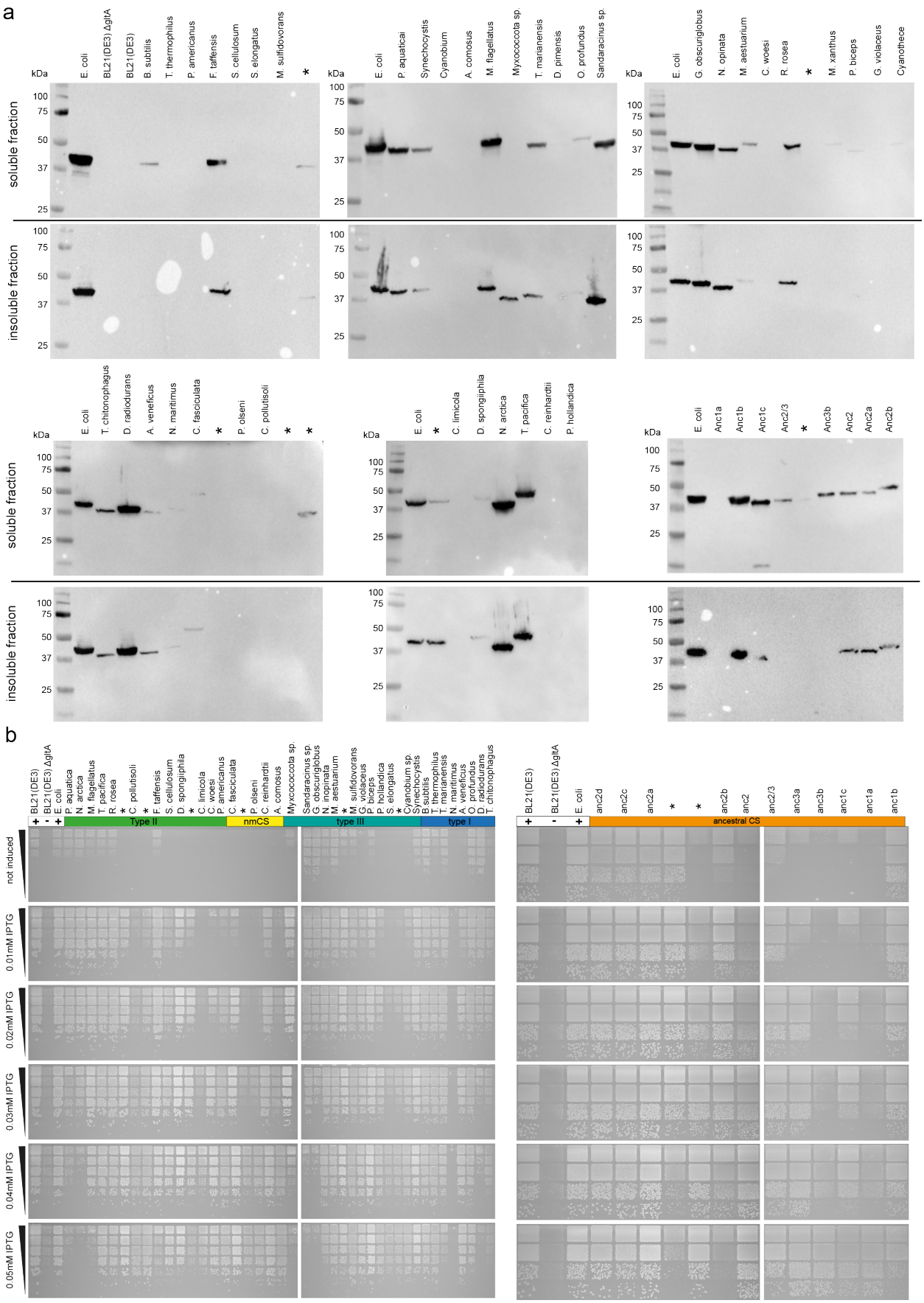
a
soluble fraction
insoluble fraction
kDa
100
75
50
37
25
E. coli
BL21(DE3) ΔgltA
BL21(DE3)
B. subtilis
T. thermophilus
P. americanus
F. taffensis
S. cellulosum
S. elongatus
M. sulfidovorans
*
P. aquaticai
Synechocystis
Cyanobium
A. comosus
M. flagellatus
Myxococcota sp.
T. marianensis
D. pimensis
O. profundus
Sandaracinus sp.
G. obscuriglobus
N. opinata
M. aestuarium
C. woesi
R. rosea
M. xanthus
P. biceps
G. violaceus
Cyanothece
T. chitonophagus
D. radiodurans
A. venefícus
N. maritimus
C. fasciculata
P. olseni
C. pollutisoli
C. limicola
D. spongiiphila
N. arctica
T. pacifica
C. reinhardtii
P. hollandica
Anc1a
Anc1b
Anc1c
Anc2/3
Anc3b
Anc2
Anc2a
Anc2b
b
not induced
0.01mM IPTG
0.02mM IPTG
0.03mM IPTG
0.04mM IPTG
0.05mM IPTG
BL21(DE3)
BL21(DE3) ΔgltA
E. coli
P. aquatica
N. arctica
M. flagellatus
T. pacifica
R. rosea
C. pollutisoli
F. taffensis
S. cellulosum
D. spongiiphila
C. limicola
C. woesi
P. americanus
C. fasciculata
P. olseni
C. reinhardtii
A. comosus
Myxococcota sp.
Sandaracinus sp.
G. obscuriglobus
N. inopinata
M. aestuarium
M. sulfidovorans
G. violaceus
P. biceps
P. hollandica
S. elongatus
Cyanobium sp.
Synechocystis
B. subtilis
T. thermophilus
T. marianensis
N. maritimus
A. venefícus
O. profundus
D. radiodurans
T. chitonophagus
Type II
nmCS
type III
type I
anc2d
anc2c
anc2a
anc2b
anc2
anc2/3
anc3a
anc3b
anc1c
anc1a
anc1b
ancestral CS

Supplementary Fig. 14 Protein production and complementation on solid media (a) Western Blots depicting the citrate synthase (CS) protein production of all tested extant and ancestral CS enzymes in *E. coli*. Comparison of protein content in the soluble and insoluble fraction after cell lysis. (b) Spot-assays of complemented *E. coli* BL21(DE3) ΔgltA strains. Cultures were spotted in a five-step serial dilution using a ratio of 1:5 for each step and incubated on M9-solid media supplemented with glucose and different Isopropyl β- d-1-thiogalactopyranoside (IPTG) concentrations. One representative plate is shown for each experiment, out of a total of three replicates for each plate.

Supplementary Table 1 Data collection and refinement statistics for the crystal structure of *M. sulfidovorans* citrate synthase (CS)

	CS from *M.sulfidovorans* PDB 8QWB
Wavelength (Å)	0.9762
Resolution range (Å)	48.31 - 3.201 (3.316 - 3.201)
Space group	P 1 21 1
Unit cell (Å)	155.69 96.61 203.1 90 110.41 90
Total reflections	636593 (60352)
Unique reflections	92644 (9175)
Multiplicity	6.9 (6.6)
Completeness (%)	98.85 (97.95)
Mean I/sigma(I)	10.32 (0.88)
Wilson B-factor	114.97
R_{merge}	0.1319 (2.263)
R_{meas}	0.1428 (2.457)
R_{pim}	0.05402 (0.9447)
CC1/2	0.998 (0.467)
CC*	1 (0.798)
Reflections used in refinement	92635 (9161)
Reflections used for R-free	4635 (459)
R_{work}	0.3252 (0.4478)
R_{free}	0.3245 (0.4490)
CC (work)	0.890 (0.463)
CC (free)	0.883 (0.481)
Number of non-hydrogen atoms	30067
macromolecules	30067
Protein residues	3816
R.m.s. deviation	
Bond lengths (Å)	0.012
Bond **angles** (°)	1.35
Ramachandran favored (%)	93.70
Ramachandran allowed (%)	6.22
Ramachandran outliers (%)	0.08
Rotamer outliers (%)	2.84
Clashscore	28.54
Average B-factor (Å^2)	134.04
M**acromolecules** (Å^2)	134.04

Statistics for the highest-resolution shell are shown in parentheses.

Supplementary Table 2 Cryo-EM data collection, refinement, and validation statistics of non-mitochondrial citrate synthase (CS) from *A. comosus*

	CS *A. comosus* **PDB 8QZP** **EMD-18779**
Data collection and Processing	
Microscope	Titan Krios
Voltage (keV)	300
Camera	Gatan K3
Magnification	29,000X
Pixel size at detector (Å/pixel)	1.09
Total electron exposure ($e^-/Å^2$)	55
Exposure rate (e^-/pixel/sec)	4.5
Number of frames collected during exposure	30
Defocus range (μm)	-3.0 to -0.5
Automation software	SerialEM
Micrographs collected (no.)	4,294
Micrographs used (no.)	1,600
Total extracted particles (no.)	587,742
Reconstruction	
Refined particles (no.)	372,284
Final particles (no.)	108,304
Symmetry imposed	C1
Resolution (global, Å)	
FSC 0.143 (unmasked/masked)	4.1/4.8
Resolution range (local, Å)	53.9 to 2.3
Map sharpening *B* factor ($Å^2$)	-222.5
Map sharpening methods	Global B factor
Model composition	
Protein	CS A. comosus
Model Refinement	
Real space refinement software	PHENIX v1.19.2
Model-Map scores (CC_mask)	0.75
B factors ($Å^2$)	(min/max/mean)
Protein	30.00/329.44/169.74
R.m.s. deviations from ideal values	
Bond lengths (Å)	0.005
Bond angles (°)	0.797
Validation	
MolProbity score	2.41
CaBLAM outliers	3.76
Clashscore	22.20
Poor rotamers (%)	1.23
Cβ outliers (%)	0.00
EMRinger score	0.30
Ramachandran plot	
Favored (%)	91.49
Allowed (%)	7.98
Outliers (%)	0.52

Supplementary Table S3 Kinetic enzyme parameters of *D. pimensis* citrate synthase and isolated size exclusion chromatography fractions containing different oligomeric state distributions

	k_{cat} (s^{-1})	K_m oxaloacetate (µM)
D. pimensis **– non-fractionated**	36.6 ± 1.1	25.4 ± 3.1
F1	39.9 ± 1.3	29.6 ± 3.9
F2	23.2 ± 0.6	15.0 ± 1.8
F3	16.6 ± 0.5	17.7 ± 2.5
F4	18.4 ± 0.6	18.4 ± 2.5
F5	14.2 ± 0.7	25.9 ± 5.0

Measurements were performed at 25 °C. N=3 technical replicates, errors = SEM

Supplementary Table 4 Kinetic characterization for different extant and ancestral citrate synthases and their variants

	aceytlCoA		oxaloacetate	
	k_{cat} (s^{-1})	$K_m$acetyl-CoA (μM)	k_{cat} (s^{-1})	$K_m$oxaloacetate (μM)
anc_{3a}	9.1 ± 0.3	22.4 ± 2.6	10.3 ± 0.1	23.9 ± 1.1
anc_{3b}	5.6 ± 0.2	8.6 ± 1.9	7.5 ± 0.2	13.2 ± 2.2
anc_{3a+5}	21.9 ± 0.8	56.5 ± 6.8	23.3 ± 61.1	61.1 ± 10.2
M. sulfidovorans WT	42.4 ± 1.0	127.4 ± 7.7	33.3 ± 1.8	50.5 ± 5.2
M. sulfidovorans W150A	34.1 ± 1.0	104.7 ± 8.9	26.7 ± 1.1	36.7 ± 5.7
A. comosus WT	41.1 ± 1.5	13.2 ± 2.3	49.2 ± 2.2	72.1 ± 10.1
A. comosus Δ487-513	41.8 ± 1.5	11.3 ± 2.0	58.9 ± 2.6	87.2 ± 11.7

Measurements were performed at 25 °C. N=3 technical replicates, errors = SEM